A R C H I V E S O F M E T A L L U R G Y A N D M A T E R I A L S
Volume 56 2011 Issue 4
DOI: 10.2478/v10172-011-0126-5

B. WODECKA-DUŚ*, D. CZEKAJ*

SYNTHESIS OF $0.7BiFeO_3$–$0.3BaTiO_3$ CERAMICS: THERMAL, STRUCTURAL AND AC IMPEDANCE STUDIES

OTRZYMYWANIE I WŁAŚCIWOŚCI DIELEKTRYCZNE CERAMIKI $0{,}7BiFeO_3$–$0{,}3BaTiO_3$

In a present paper results of the process of synthesis and study of a perovskite-type solid solution of the chemical composition (1-x)$BiFeO_3$–$xBaTiO_3$ for x=0.3 are reported. Synthesis of $0.7BiFeO_3$–$0.3BaTiO_3$ (BF–BT) ceramics was carried out according to the solid-phase reaction from the mixture of powders. Simultaneous thermal analysis (STA) and X-ray diffraction method were utilized to study the synthesis of BF–BT ceramics. On the basis of STA analysis the optimum conditions of the thermal treatment were found. BF–BT ceramics was studied in terms of its microstructure (SEM), chemical composition (EDS), crystalline structure (XRD), and dielectric properties (impedance spectroscopy) at room temperature. It was found that dense BF–BT ceramics with a cubic structure of *Pm3m* space group and desired stoichiometry (±3%) was fabricated under technological conditions differing in both sintering temperature (T=750°C–850°C) and soaking time (t=2h-40h). It was found that an increase in sintering temperature for ΔT=100°C made it possible to decrease the soaking time 10 times. Impedance spectroscopy was utilized for characterizing dynamical dielectric properties of 0.7BF–0.3BT ceramics. The alternative representation of impedance data in a form of complex plot (Z'' vs. Z') as well as simultaneous Bode plots (imaginary parts of impedance Z'', admittance Y'', electric modulus M'' and tanδ versus frequency in a log-log scale) were used for preliminary visual analysis. Kramers-Kronig transform test was utilized for experimental data validation. To analyze the room temperature impedance spectroscopy data complex nonlinear least squares fitting method was used and the data were fitted to the corresponding equivalent circuit consisting of resistors and constant phase elements. Agreement between experimental and simulated data was established.

Keywords: dielectric properties, impedance spectroscopy, $BiFeO_3$–$BaTiO_3$, ceramics

W niniejszej pracy przedstawiono rezultaty badań poświęconych wytwarzaniu i charakterystyce właściwości roztworu stałego o strukturze typu perowskitu i składzie chemicznym (1-x)$BiFeO_3$–$xBaTiO_3$ dla x=0,3. Proces syntezy ceramiki $0{,}7BiFeO_3$–$0{,}3BaTiO_3$ (BF-BT) przeprowadzono w wyniku reakcji w fazie stałej z mieszaniny prostych tlenków. Przy pomocy analizy termicznej (STA) oraz rentgenowskiej analizy strukturalnej dokonano charakterystyki procesu syntezy ceramiki BF-BT. Przeprowadzono badania mikrostruktury ceramiki BF-BT za pomocą skaningowego mikroskopu elektronowego (SEM), określono stechiometrię składu chemicznego przy użyciu metody EDS, a strukturę krystaliczną badano metodą dyfrakcji rentgenowskiej (RTG). Przeprowadzono badania właściwości dielektyrcznych wytworzonej ceramiki metodą spektroskopii impedancyjnej. Wykorzystując metodę swobodnego spiekania dla trzech różnych warunków technologicznych (T=750-880°C, t=2-40h) otrzymano ceramikę 0,7BF–0,3BT o dużej czystości i homogeniczności składu (±3%), wykazującą strukturę regularną *Pm3m*. Na podstawie przeprowadzonych badań stwierdzono, iż zwiększenie temperatury syntezy i spiekania o ΔT=100°C, pozwoliło zmniejszyć czas wytrzymania ceramiki 10 razy. Badania przeprowadzone metodą spektroskopii impedancyjnej pozwoliły na scharakteryzowanie właściwości dielektrycznych ceramiki 0,7BF–0,3BT. Dane impedancyjneprzedstawiono w płaszczyźnie zespolonej Z'' od Z' oraz w postaci zależności częstotliwościowych urojonych składowych impedancji $Z''(\nu)$, modułu elektrycznego $M''(\nu)$, admitancji $Y''(\nu)$ i strat dielektrycznych tg$\delta(\nu)$. Spójność danych pomiarowych sprawdzono przy pomocy metodyki Kramersa-Kroniga, która potwierdziła poprawność danych eksperymentalnych.

1. Introduction

Multiferroic materials exhibit two or more of ferroelectricity, ferromagnetism (or antiferromagnetism), and ferroelasticity. Materials that exhibit both ferroeleasticity and ferroelectricty or ferromagnetism are relatively well known. However, only a limited number of materials are both ferroelectric and ferromagnetic [1,2]. These magnetoelectric multiferroic materials are both of theoretical interest, in elucidating just why they are so scarce, and of practical interest, in for example the application in memory devices [3] or actuators/transducers [4].

* UNIVERSITY OF SILESIA, DEPARTMENT OF MATERIALS SCIENCE, 41-200 SOSNOWIEC, 2 ŚNIEŻNA STR., POLAND

Materials in which (anti-)ferroelectricity, (anti-)ferromagnetism and ferroelasticity coexist simultaneously are referred to as "multiferroics" and have been intensively studied because of their potential applications in information storage and sensors [5,6]. The use of multiferroic ceramics or mixed ferroelectric-ferromagnetic systems is nowadays a field of great interest due to the possibility of having double excitation source sensors and actuators. The most widely studied systems belong to the families of cobalt and nickel ferrites combined with ferroelectrics like $BaTiO_3$ [7] or piezoelectrics like $Pb(Zr,Ti)O_3$ [8]. One of the main applications for these materials is due to the magnetoelectricity [9,10].

$BiFeO_3$ is a typical multifferoic material in which ferroelectricity and anti-ferromagnetism coexist at room temperature [11]. $BiFeO_3$ forms solid solutions with a number of other perovskites of ABO_3 type (Fig.1). It is reported in literature that when forming solid solutions, $BiFeO_3$ exhibits different structural transformations, with increasing content of the second phase.

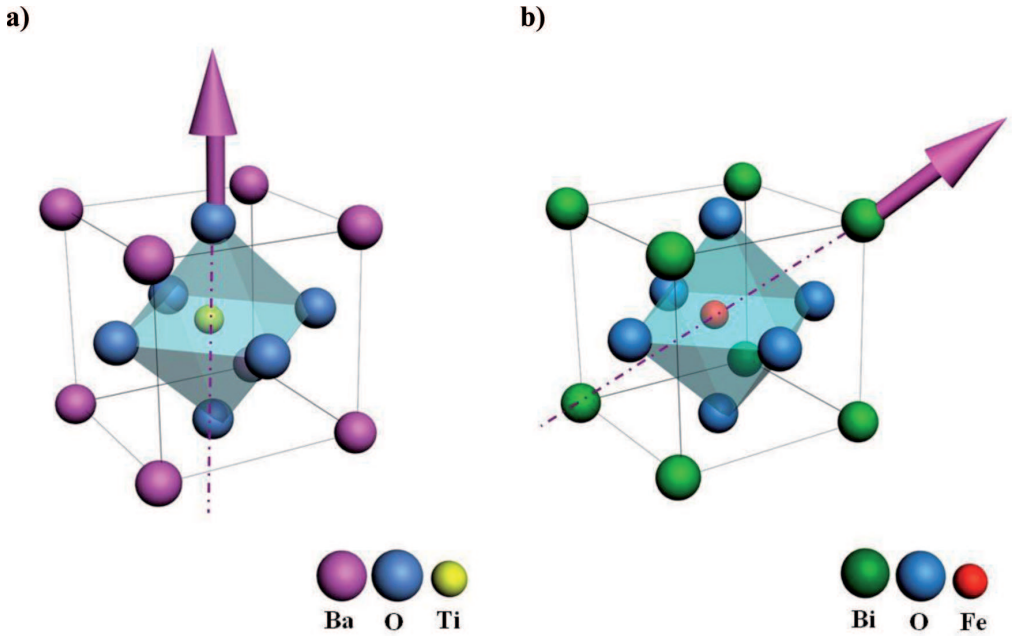

Fig. 1. Perovskite-type structure ABO_3 of $BaTiO_3$ adopting tetragonal symmetry (a) and $BiFeO_3$ exhibitibng rhombohedral symmetry (b). Direction of the polarization vector P is also shown

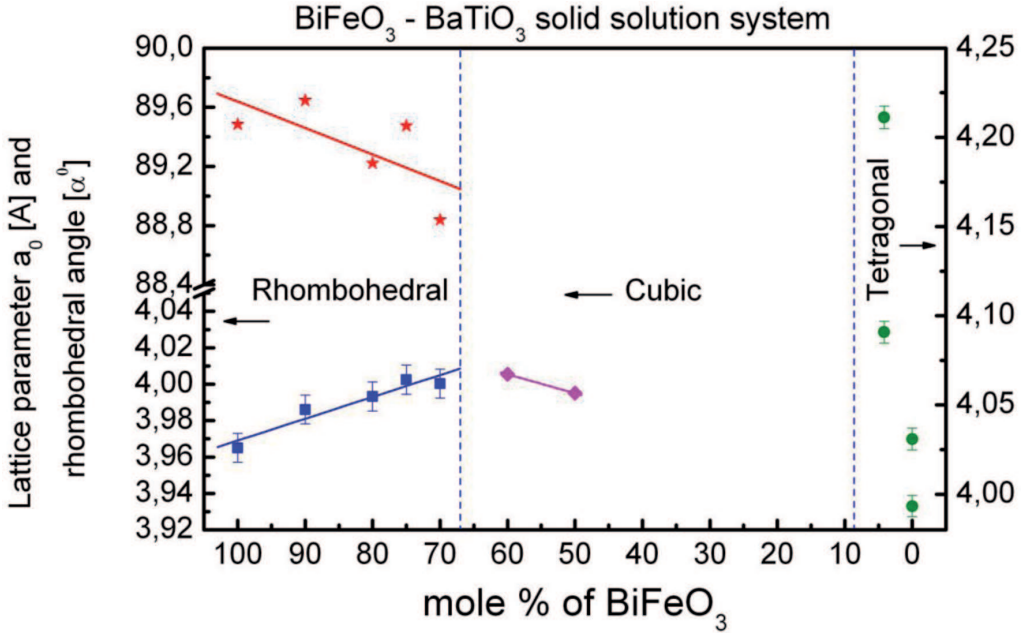

Fig. 2. Phase diagram of $BiFeO_3$–$BaTiO_3$ - prepared on the base of data from [12,13]

On the basis of the up-to-date experimental results an attempt was made to draw a phase diagram for the solid solution system $BiFeO_3$–$BaTiO_3$ (Fig. 2). It results from that phase diagram that the rhombohedral symmetry is dominating in the $BiFeO_3$ rich phases and it lasts up to 68 mole% of $BiFeO_3$. With an increase in amount of $BaTiO_3$ component the rhombohedral lattice parameter a shows an increase while the rhombohedral angle α shows a decrease. The phase boundary between the rhombohedral and the cubic phases was found to be at about 68 mole% of $BiFeO_3$. In the cubic phase, the lattice parameter slightly decreases. The phase boundary between the cubic and the rhombohedral phase was marked for about 8 mole% of $BiFeO_3$. Also one can see in that diagram the lattice parameters of the end compounds [12,13].

It was our goal in the present study to investigate the process of synthesis of $0.7BiFeO_3$–$0.3BaTiO_3$ ceramics by simultaneous thermal analysis (STA) as well as to study its structure, microstructure and basic dielectric properties with impedance spectroscopy.

2. Experiment

Ceramic solid solution samples under study are $(1\text{-}x)BiFeO_3$–$xBaTiO_3$ where x=0.3 (0.7BF–0.3BT). The samples were synthesized using solid state reaction method, using oxides Bi_2O_3 (99.9% Aldrich), Fe_2O_3, TiO_2 (>99% Fluka) and carbonate $BaCO_3$ (99.99% POCh) in appropriate proportions (mixed oxide method MOM).

To reveal characteristic features of the synthesis of $0.7BiFeO_3$–$0.3BaTiO_3$ ceramics the stoichiometric mixture of powders corresponding to the chemical solid-phase reaction given below:

$$0.35Bi_2O_3 + 0.35Fe_2O_3 + 0.3BaCO_3 + 0.3TiO_2 \rightarrow 0.7BiFeO_3 - 0.3BaTiO_3 + 0.3CO_2 \uparrow \quad (1)$$

were thoroughly prepared.

To obtain a homogeneous mixture stoichiometric amounts of oxide and carbonate precursors were weighted and mixed thoroughly in a zirconate mortar. Then they were milled for 24h and calcined at various temperatures within the range T=750-850°C for t=2-20h. The calcined powders were ground thoroughly and milled again and the powders were pressed into compacts in a stainless-steel die at the pressure of p=300MPa so the pellets of d=10mm in diameter and$h$=1mm in thickness were formed.

Final sintering temperatures were chosen from the range T=780-880°C keeping in mind the high formation temperature of 0.7BF–0.3BT. The soaking time was t=4-40h and the heating rate for each firing was chosen as 5°C/min which has been reported to be slow enough to produce high density ceramics with small phase transition broadening. Table 1 gives the final sintering temperatures adopted in the present research.

TABLE 1
The final sintering temperatures adopted

Methods	Synthesis I	Synthesis II	Final sintering	Annealed in air
Method I	750°C/20h	750°C/20h	780°C/40h	550°C/10h
Method II	800°C/10h	800°C/10h	830°C/20h	550°C/10h
Method III	850°C/2h	850°C/2h	880°C/4h	550°C/10h

Simultaneous thermal analysis (STA), in which both thermal analysis (DTA) and mass change effects (TG and DTG) are measured concurrently on the same sample was used to investigate both synthesis effects in the stoichiometric mixture of powders. The measurements were obtained with Netzsch STA409 thermal analyzer which is a combined DTA/TG/DTG system.

Microstructure was investigated by scanning electron microscope (FESEM) HITACHI S-4700 and the chemical composition was studied with an energy dispersive spectrometer (EDS) NORAN Vantage.

The crystal structure of bulk ceramics were studied by X-ray diffraction method at room temperature (XRD diffractometer, Philips PW 3710, CoK_α radiation).

Electrodes for electrical measurements of the ceramic samples were fabricated from silver paste. The dielectric properties of 0.7BF–0.3BT ceramics were studied by impedance spectroscopy with a Quadtech 1920-type precision LCR meter within the frequency range ν=10Hz-1MHz at room temperature.

3. Results and discussions

Powdered stoichiometric mixture of oxides conveponding to $0.7BiFeO_3$–$0.3BaTiO_3$ solid solutions was investigated by STA within the temperature range T=20-1300°C. One can see in Fig. 3 the traces of DTA, TG and DTG recorded at heating rate 10deg/min.

As result of the thermogravimetric measurements the specific temperature ranges corresponding to different rates of the chemical reaction have been stated. Temperature of synthesis was chosen as T=800°C – which corresponds to the end of the mass changes effects (i.e., saturation of the TG-curve, Fig. 3). Also the temperature at which the chemical reaction runs at maximal rate was determined T=727.9°C (i.e., the peak at DTG curve, Fig. 3). One can see in Fig. 4 that the mass loss of the stoichiometric mixture of oxides,

viz. Bi_2O_3, Fe_2O_3, TiO_2, $BaCO_3$ changes in a two – step way within the temperature range ΔT=390-800°C and reaches a value of Δm ≈4.61%. The first step of a mass loss (Δm ≈0.04%) takes place within the temperature range ΔT=390°C-450°C and exhibits the highest rate at T=392°C (peak at DTG curve, Fig. 3) and is due to the organic impurities evaporation. The second step, taking place within the temperature range ΔT=650-800°C is accompanied with the larger mass loss of about Δm ≈4.57% (the highest rate of the mass loss was found at T=727.9°C). One can ascribe this mass change effect to formation of the desired perovskite – type phase with CO_2 evaporation. Results of the differential thermal analysis of 0.7BF–0.3BT ceramic powder, given in Fig. 3 and Fig. 4 show the presence of a sharp endothermic peak at T=1202.9°C. It should be noted that no mass change effects occur at this temperature region. Therefore, this endothermic peak can be ascribed to the solidus temperature of the synthesized material.

On the base of results of the simultaneous thermal analysis (Fig. 3 and Fig. 4) the temperature regimes for the technological process of 0.7BF–0.3BT ceramics fabrication have been determined.

Both point and surface EDS analysis have been performed for 0.7BF–0.3BT ceramics. They have proved conservation of the chemical composition of the material under studies. Results of EDS analysis performed for 0.7BF–0.3BT ceramics sintered at different technological conditions are given in Fig. 5. The insets in Fig. 6 show photographs of the microstructure of ceramics. One can see that an increase in temperature of sintering causes formation of homogeneous, non-porous, well-formed grain microstructure.

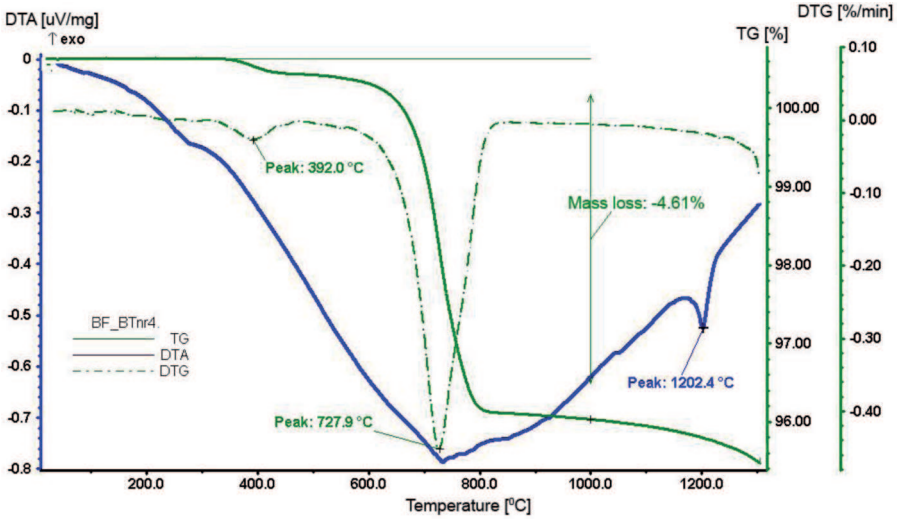

Fig. 3. Results of simultaneous thermal analysis of stoichiometric mixture of oxides

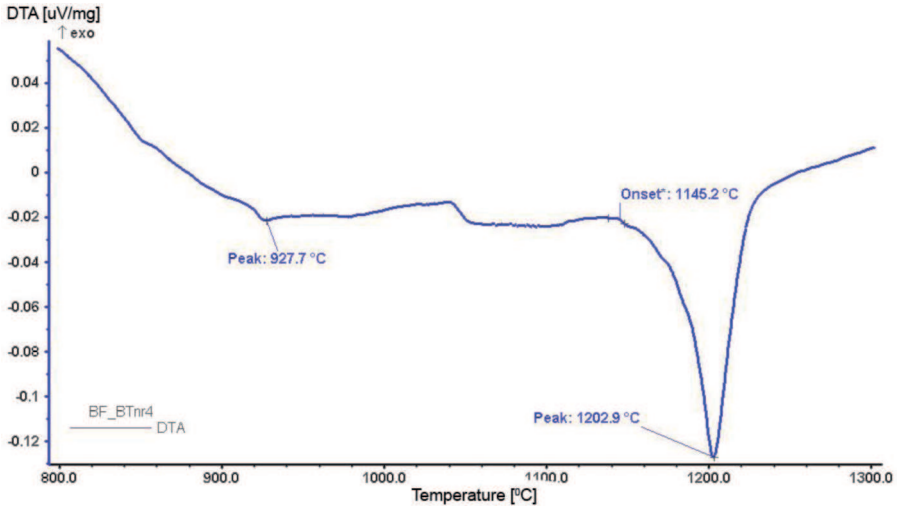

Fig. 4. DTA curve registered for stoichiometric mixture of oxides within temperature range ΔT=800-1300°C

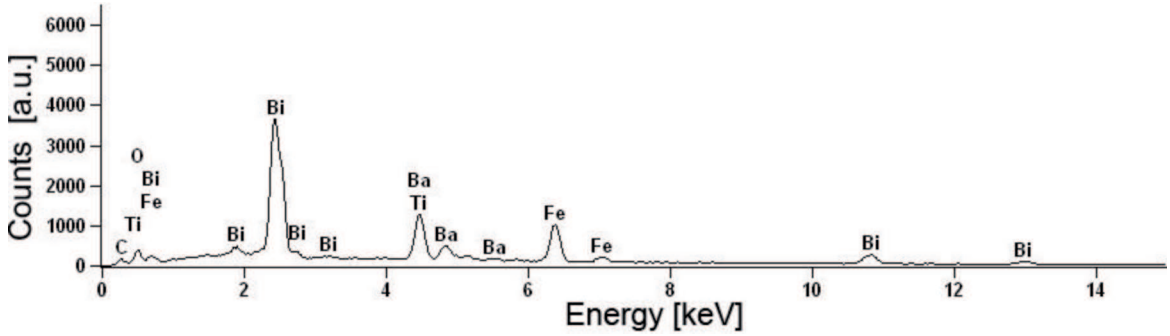

Fig. 5. EDS spectrum of $0.7BiFeO_3$–$0.3BaTiO_3$ ceramics

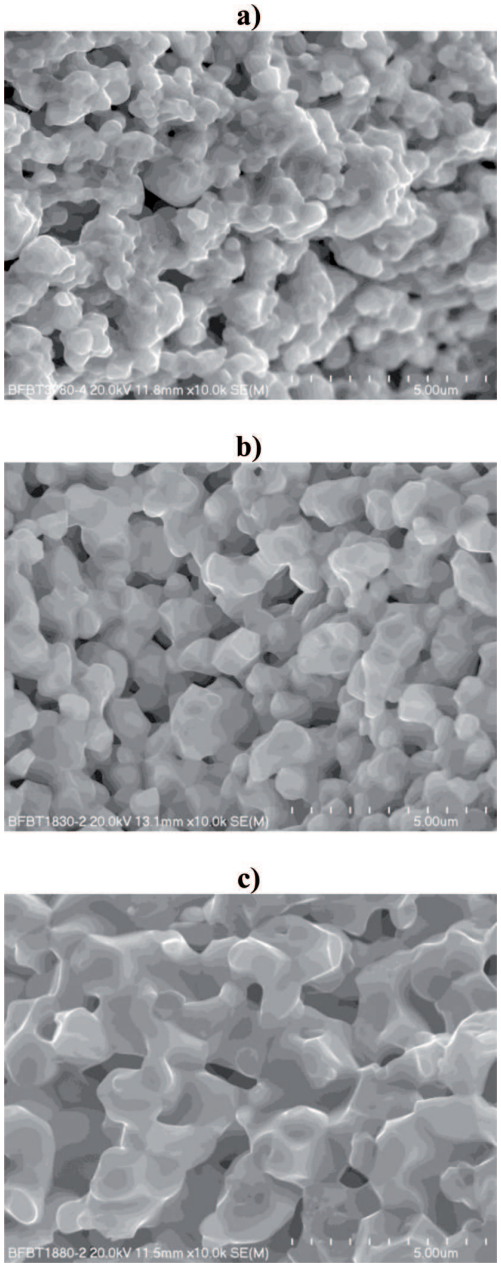

Fig. 6. SEM photographs of the microstructure fracture of $0.7BiFeO_3$–$0.3BaTiO_3$ ceramics specimens: (a) sintered at T=780°C, (b) sintered at T=830°C, (c) sintered at T=880°C (x10 000)

Quantitative analysis of the chemical composition was performed with a Noran Vantage software. Results of the calculations are given in Table 2. One can see that small deviations from the theoretical composition of 0.7BF–0.3BT have occurred but they do not exceed a value of ±3% what is consistent with the resolution of the utilized method of investigation.

TABLE 2
Theoretical and experimental content of elements (calculation for simple oxide) for $0.7BiFeO_3$–$0.3BaTiO_3$ ceramic

Formula	Theoretic contents of oxides [%]	Contents of oxides from EDS [%] (measurement)	Accuracy [%]
TiO_2	8.29	8.11	2
Fe_2O_3	19.34	19.19	2
BaO	15.92	16.74	5
Bi_2O_3	56.44	55.96	1

The X-ray diffraction analysis was performed at room temperature and formation of the desired crystalline structure has been confirmed. A careful examination of the X-ray diffraction patterns performed with the help of X'Pert HighScore Plus software (PANalytical, B.V) indicated that no preferred orientation was present at any sample under investigation. Results of the X-ray phase analysis of 0.7BF–0.3BT ceramics have shown the presence of one phase only for all technological methods utilized in the present study.

The lattice parameters for 0.7BF–0.3BT ceramics were calculated on the base of X-ray diffraction pattern. The Rietveld refinement method, embedded into utilized computer programme has been used for calculating parameters of the cubic elementary cell. A model structure used for the diffraction pattern fitting exhibited a *Pm3m* space group (SG number: 221) (Fig.7). All calculated parameters of the Rietveld refinement i.e. parameters of the cubic elementary cell (a_0), volume of the elementary cell (V), calculated density (ρ) mean volume of the crystallite size (D) and lattice strain (ε) are given in Ta-

ble 3. One can see in Tab. 3 that values of the Rietveld *R*-factor prove a good quality of the fitting process. It follows from Table 3 that technological methods used in the present study do not influence much on a change of the crystallographic parameters of 0.7BF–0.3BT ceramics. However, one can see that an increase in temperature of sintering and a decrease in the sintering time cause a small decrease in the elementary cell volume, as well as a small increase in the calculated density. An increase in temperature of sintering of $0.7BiFeO_3$–$0.3BaTiO_3$ ceramics for 100°C and a decrease in a soaking time for 10 times causes an increase in a mean dimension of crystallites for 24% and a decrease in a lattice strain for 19% (Table 3).

It is commonly known [14-16], that impedance spectroscopy (IS) is a powerful method of characterizing many of the electrical properties of materials and their interfaces with electronically conducting electrodes. With an appropriate data analysis, it is often possible to characterize the different electrically active regions in a material by demonstrating their existence and by measuring their individual electric properties [15].

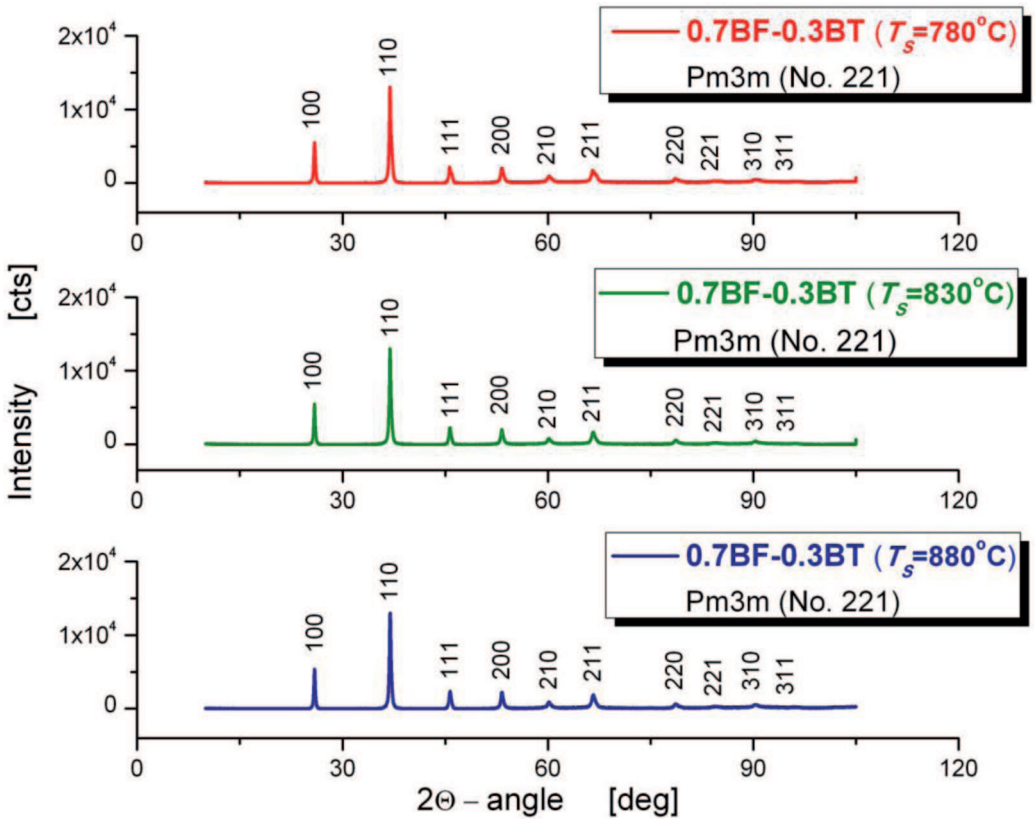

Fig. 7. Comparison of X-ray diffraction patterns for 0.7BF–0.3BT ceramics fabricated of different technological conditions (T_S- sintering temperature)

TABLE 3

Crystallographic parameters of 0.7BF–0.3BT ceramics fabricated at different technological conditions

Methods	a_0 **[nm]**	$V \cdot 10^{30}$ **[m^3]**	ρ **[kg/m^3]**	D **[Å]**	ε **[%]**	**Rietveld *R*-factors**		
						R_p	R_{wp}	R_{exp}
Method I	0.399(2)	63.60	6089	269.2	0.141	4.07	6.36	1.53
Method II	0.399(1)	63.57	6091	278.7	0.136	5.14	9.53	1.53
Method III	0.399(0)	63.54	6094	333.0	0.114	3.44	5.06	1.56

The frequency dependent properties of a material are normally described in terms of any of the formalism expressed as,
complex impedance:

$$Z^* = Z' - jZ'' = \frac{1}{Y^*} = R_S - \frac{j}{j\omega C_S} \tag{2}$$

complex admittance:

$$Y^* = \frac{1}{R_p} + j\omega C_p \tag{3}$$

complex permittivity:

$$\varepsilon^* = \varepsilon' - j\varepsilon'' \tag{4}$$

complex modulus:

$$M^* = M' + jM'' = \frac{1}{\varepsilon^*} = j\omega C_0 Z^* \tag{5}$$

where subscripts p and s refer to equivalent parallel and series circuit components, $\omega=2\pi\nu$, angular frequency, C_0 is capacitance of the cell in vacuum (Z', Y', ε', M') and (Z'', Y'', ε", M'') are the real and imaginary components of impedance, admittance, permittivity, and modulus, respectively.

The above expressions are interrelated with each other and offer a wide scope for graphical representation. Each representation can be used to highlight a particular aspect of the response of a sample. The idealized plot (Z''vs. Z'), which describes a polycrystalline oxide material, often includes three components with their corresponding relaxation frequencies. At higher frequencies, the component normally corresponds to the bulk properties (ν_b), at intermediate frequency the element corresponds to the grain boundaries (ν_{gb}), and at low frequency, we usually have the electrode processes (ν_{el}) or processes occurring at the material/ electrode interface. Typically, ν_b is one or two orders of magnitude higher than ν_{gb} and ν_{el} is much smaller than ν_{gb} ($\nu_{el} \ll \nu_{gb} \ll \nu_b$). In real oxide systems this behavior may be rather complicated due to the different factors which influence the bulk and the grain boundary properties-chemical composition, impurities, ageing, and technological conditions. When overlapping between processes increases, one may need alternative representations [17,18].

Alternative representation of the impedance data in a form of simultaneous frequency dependence of imaginary part of impedance Z'', admitance Y'', electric modulus M'' and dielectric loss tangent tanδ for 0.7BF–0.3BT ceramics sintered under different technological conditions is given in Fig. 8.

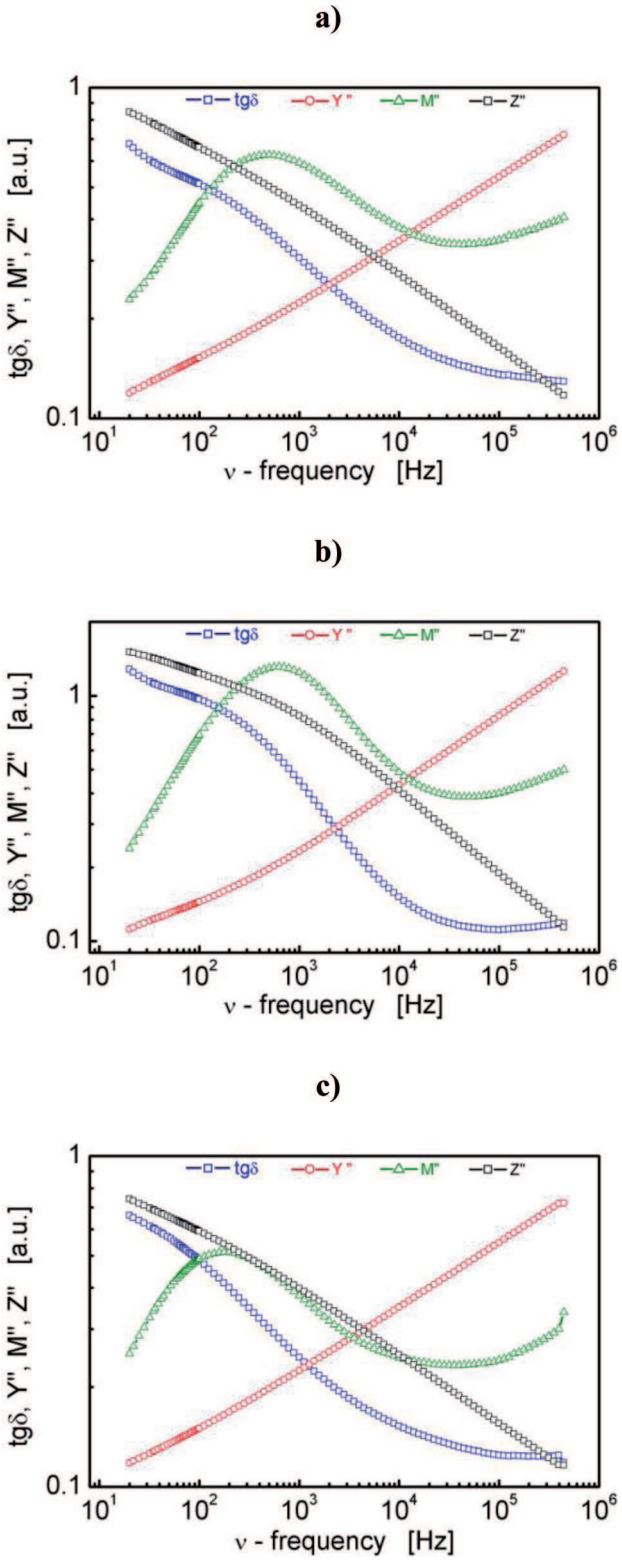

Fig. 8. Dependence of imaginary part of impedance (Z''), admittance (Y''), electric modulus (M'') and dielectric loss tangent (tanδ) on frequency for 0.7BF–0.3BT ceramic: (a) sintered at T=780°C (method I), (b) sintered at T=830°C (method II), (c) sintered at T=880°C (method III)

One can see that in a log-log scale experimental data form smooth curves that monotonously increase (Y'' curve) or decrease (Z'' curve) with an increase in mea-

suring frequency or reach local minima or maxima (both M'' and tanδ curves). These alternative representations may be used to interpret the impedance spectra of polycrystalline materials. The representation of log(Z'') vs. log(ν) is suitable for the most resistive contributions, but may be insufficient for minor terms such as the bulk contribution with very resistive grain boundaries and for cases when the bulk and grain boundary arcs overlap. In these cases, the modulus representation, log(M'') vs. log(ν), is suitable for the bulk contribution and/or other contributions with low capacity; however, it may not reveal contributions with higher capacity. In this case, the alternative representation of log(tan(δ)) vs. log(ν) may be more useful for an overall analysis of impedance spectra. The peaks of this representation yield the relaxation frequencies, and the minima can be related to the transitions from bulk to grain boundary and grain boundary to electrode [17,19]. The identification of the peaks and minima obtained from simultaneous representations of impedance data may be an alternative to well-known computer programs [15] or one may also use the parameters extracted from the actual representations of log(Z''), log(M''), and log(tan(δ)) as initial parameters to assist the convergence of computer codes [14].

To check the quality of the impedance data, what is essential for a proper complex nonlinear least squares (CNLS) analysis, the Kramers-Kronig (K-K) validation tests were performed with the use of computer program by Boukamp [15,16]. Details of the method used are given elsewhere [15,18]. In the present research results of the K-K test in a form of the relative differences plot are given in Fig. 9-11 as insets. A random distribution of the real part relative differences (circles) and the imaginary part differences (open squares) between the measured and calculated values (residuals) around the frequency axis indicates that the data are K-K compliant [17]. The resulting "pseudo Chi-squared" value is shown in Fig. 9-11.

Ceramic materials are composed of grains separated by grain boundaries with different resistivities. The grain and grain boundary contribution to the resistivity can be visualized by considering capacitance and resistance with various configurations. The promising way to understand these contributions is to study a complex impedance spectra of the samples and compare these plots with the complex impedance spectra of the equivalent circuit which should provide a realistic representation of the electrical analog of the ceramics.

One of the possible equivalent circuit is that the grain (bulk) and grain boundary contribution can be represented by two parallel combinations of resistance (R) and capacitance (C) connected in series. When the relaxation times of bulk and grain boundary processes differ, the output response which, when plotted in a complex plane plot (Z'' vs. Z') appears in a form of succession of semicircles representing electric phenomena due to bulk material and grain boundary effect. If the relaxation times are comparable, then the semicircles overlap with one another to give a summation of the peaks.

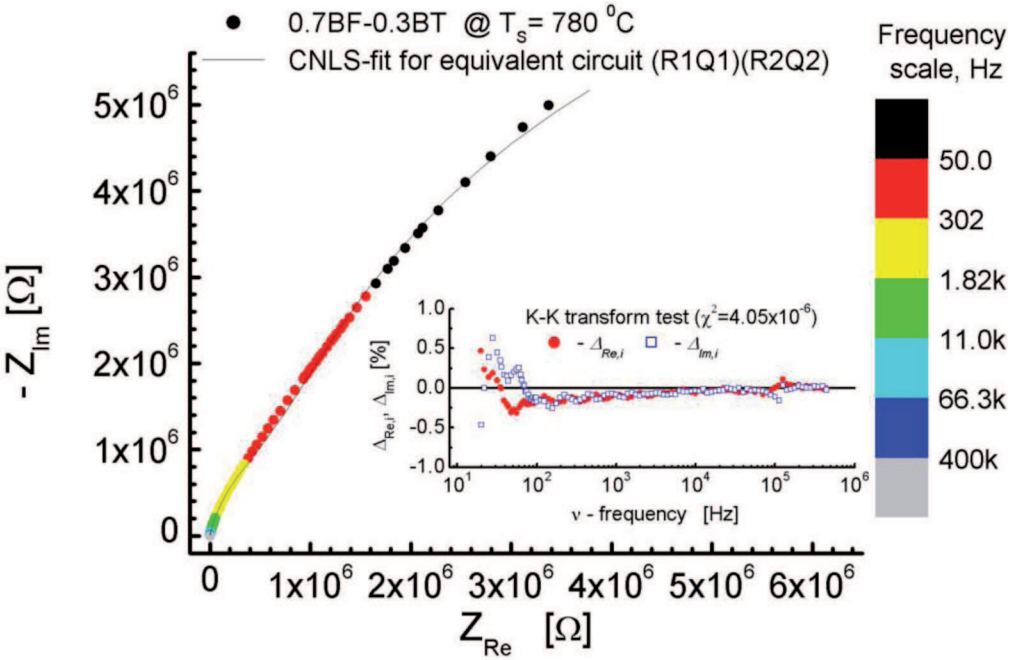

Fig. 9. Impedance diagram for 0.7BF–0.3BT ceramic sintered at T=780°C (method I) and Kramers-Kronig test of impedance date

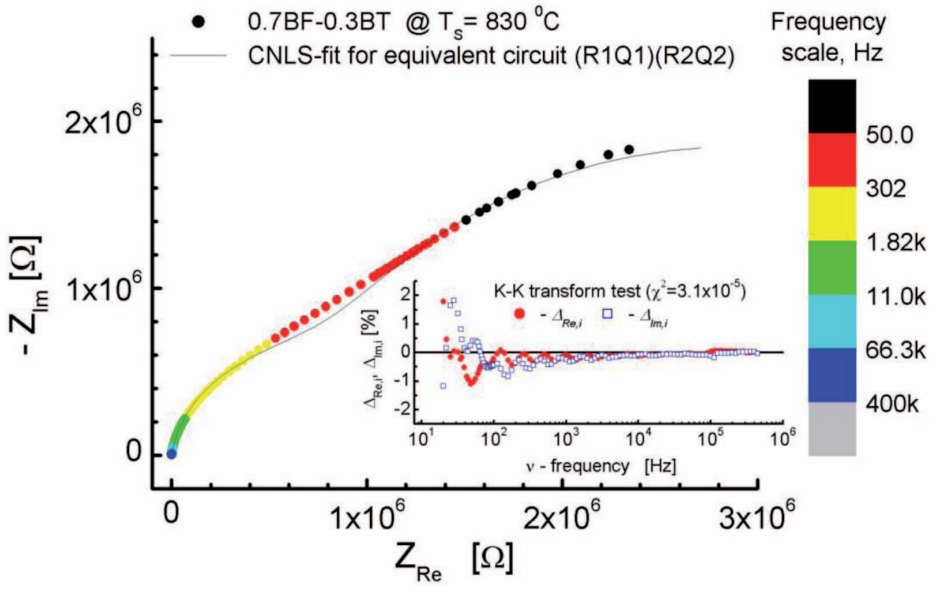

Fig. 10. Impedance diagram for 0.7BF–0.3BT ceramic sintered at T=830°C (method II) and Kramers-Kronig test of impedance date

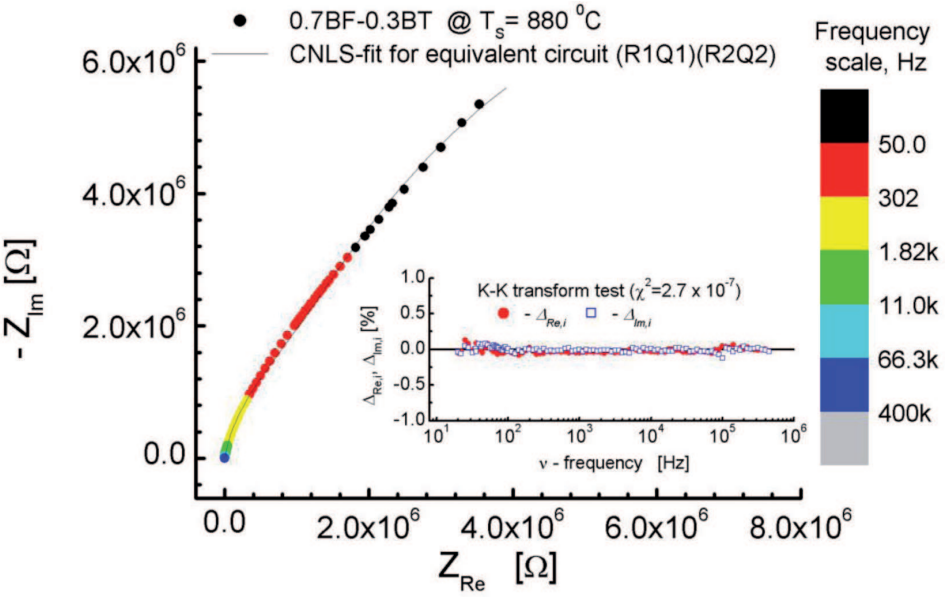

Fig. 11. Impedance diagram for 0.7BF–0.3BT ceramic sintered at T=880°C (method III) and Kramers-Kronig test of impedance date

Results of the impedance spectroscopy measurements of $0.7BiFeO_3$–$0.3BaTiO_3$ ceramics are presented in a complex plane, where imaginary part of impedance Z'' is plotted against the real part of impedance Z'. One can see in Fig. 9-11 that there is no clear appearance of semicircles. Therefore the equivalent electric circuit model used for data simulation in the present study consisted of a series combination of two parallel combinations of the resistance (R) and the constant-phase element (Q), which represents more accurately the behavior of the grain interior and grain boundary processes [15,20] (Fig. 12).

Results of the simulation performed according to the complex non-linear least squares method (CNLS, ZView program by Scribner Associates, Inc.) are given in complex plane plots (Fig. 9-11) whereas estimated parameters of the equivalent circuit are given in Tab. 4. The validity of the fitting procedure was estimated according to χ-squared and the weighted sum of squares, referred to as χ^2 and WSS, respectively (Tab. 4). In this connection it is worth noting that the estimations of the validity of the simulations are in good agreement with other published results on ceramics.

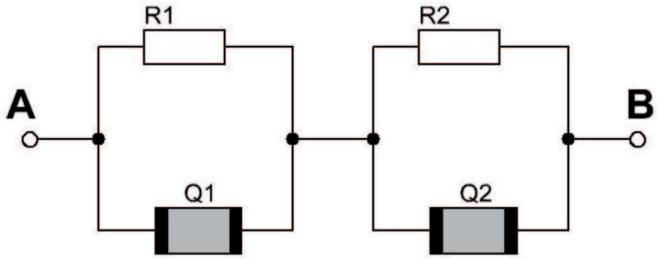

Fig. 12. Schematic representation of the equivalent circuit used in the dispersion analysis for 0.7BF–0.3BT ceramics

TABLE 4

Parameters of the electric equivalent circuit

Element	**0.7BF–0.3BT**		
Temperature	T_S**=780°C**	T_S**=830°C**	T_S**=880°C**
R1 [Ω]	$6.856 \cdot 10^5$	$7.6607 \cdot 10^5$	$1.1059 \cdot 10^6$
CPE1-T [F]	$2.1266 \cdot 10^{-9}$	$9.099 \cdot 10^{-10}$	$2.1256 \cdot 10^{-9}$
CPE1-P	0.89559	0.9323	0.89868
R2 [Ω]	$1.5195 \cdot 10^7$	$4.2732 \cdot 10^6$	$1.7235 \cdot 10^7$
CPE2-T [F]	$1.8202 \cdot 10^{-9}$	$3.4895 \cdot 10^{-9}$	$1.704 \cdot 10^{-9}$
CPE2-P	0.90514	0.89138	0.9201
χ^2	$3.864 \cdot 10^{-4}$	$8.0281 \cdot 10^{-4}$	$2.6691 \cdot 10^{-4}$
WSS	0.074961	0.15574	0.051781

4. Conclusions

In the present study 0.7BF–0.3BT ceramics has been fabricated by mixed oxide method from the stoichiometric mixture of oxides, viz. Bi_2O_3, Fe_2O_3, TiO_2 and carbonate $BaCO_3$. The simultaneous thermal analysis was used to determine the temperature regimes for the technological process. Three methods of the thermal treatment differing in sintering temperatures (T=750°C-850°C) and soaking times (t=2h-40h) were applied . It was found that an increase in sintering temperature for ΔT=100°C made it possible to decrease the soaking time 10 times and fabricate 0.7BF–0.3BT ceramics that adopted the same cubic perovskite type structure described by *Pm3m* space group (No. 221) and the lattice parameter a_0=0.399nm. Also the chemical composition of the ceramic samples prepared under different technological conditions corresponded to the theoretical one with accuracy of ±3%. However, an increase in the sintering temperature caused an increase in mean crystallite size for about 24% and a decrease in lattice strain for about 20%. Dielectric properties of BF–BT ceramics were well described by an equivalent electric circuit with two relaxation times.

Received: 20 April 2011.

Acknowledgements

The present research has been supported by Polish Ministry of Education and Science from the funds for science in 2010-2013 as a research project N N507 494338.

REFERENCES

[1] V. Fruth, L. Mitoseriu, D. Berger, A. Iancu lescu, C. Matei, S. Preda, M. Zaharescu, Progress in Solid State Chemistry **35**, 193-202 (2007).
[2] G.L. Yuan, S.W. Or, Y.P. Wang, Z.G. Liu, J.M. Liu, Solid State Communications **138**, 76-81 (2006).
[3] J.K. Kim, S.S. Kim, W.J. Kim, Materials Letters **59**, 4006-4009 (2005).
[4] T. Veno, J. Qiu, J. Tani, Journal of Magnetism and Magnetic materials **258-259**, 490-492 (2003).
[5] N. Fujimura, S. Azuma, N. Aoki, T. Yoshimura, T. Ito, J. Appl. Phys. **80**, 7084 (1996).
[6] N. Fujimura, T. Ishida, T. Yoshimura, T. Ito, Appl. Phys.Lett. **69**, 1011 (1996).
[7] B. Wodecka-Duś, D. Czekaj, Archives of Metallurgy and Materials **54**, 923-933 (2009).
[8] R. Zachariasz, D. Bochenek, Archives of Metalurgy and Materials **54**, 895-902 (2009).
[9] Y.H. Chu, L.W. Martin, M.B. Holcomb, R. Ramesh, Department of Materials Science Engineering and Department of Physics **10**, 16-23 (2007).
[10] J.S. Kim, Ch. Cheon, P.W. Jang, Y.N. Choi, C.H. Lee, Journal of the European Ceramic Society **24**, 1551 (2004).
[11] Y. Horibe, M. Nakayama, Y. Hosokoshi, T. Asaka, Y. Matsui, T. Asada, Y. Koyama, S. Mori, Japanese Journal of Applied Physics **44**, 7148 (2005).
[12] M.M. Kumar, A. Srinivas, S.V. Suryanarayana, J. Appl. Phys. **87**, 857 (2000).
[13] I.H. Ismailzade, R.M. Ismailov, A.I. Alekberov, F.M. Salaev, Phys. Status Solidi **68**, 81 (1981).
[14] E. Borsukov, J.R. Macdonald (Eds), Impedance spectroscop, John Wiley and Sons, New York (2005).
[15] D. Czekaj, A. Lisińska-Czekaj, T. Orkisz, J. Orkisz, G. Smalarz, Journal of the European Ceramic Society **30**, 465-470 (2010).
[16] B.A. Boukamp, Solid State Ionics **169**, 65-73 (2004).
[17] D.C. Sinclair, A.R. West, J. Appl. Phys. **66**, 3850-3856 (1989).
[18] H. Bernard, A. Lisińska-Czekaj, J. Dzik, K. Osińska, D. Czekaj, Archives of Metallurgy and Materials, (accepted for publication) (2011).
[19] J.C.C. Abrantes, J.A. Labrincha, J.R. Frade, Materials Research Bulletin **35**, 727-976 (2000).
[20] A. Lasia, Kluver Academic/Plenum Publishers **32**, 143-248, New York (1999).